Structure of the water ice surface studied by x-ray absorption spectroscopy at the O K-edge

Ph. Parent, C. Laffon, C. Mangeney, F. Bournel, and M. Tronc

Citation: The Journal of Chemical Physics **117**, 10842 (2002); doi: 10.1063/1.1519256
View online: http://dx.doi.org/10.1063/1.1519256
View Table of Contents: http://scitation.aip.org/content/aip/journal/jcp/117/23?ver=pdfcov
Published by the AIP Publishing

Structure of the water ice surface studied by x-ray absorption spectroscopy at the O K-edge

Ph. Parent[a] and C. Laffon
Laboratoire pour l'Utilisation du Rayonnement Electromagnétique (LURE), Centre Universitaire de Paris-Sud, Bât. 209d, BP 34, 91898 Orsay Cedex, France

C. Mangeney, F. Bournel, and M. Tronc
Laboratoire de Chimie Physique, Matière et Rayonnement, 11, rue Pierre et Marie Curie, 75231 Paris Cedex 05, France

(Received 28 March 2002; accepted 12 September 2002)

Vapor-deposited H_2O ice films grown between 38 and 150 K under ultrahigh vacuum conditions have been investigated using near-edge x-ray absorption fine structure (NEXAFS) spectroscopy at the oxygen K-edge, in conventional mode—which is bulk sensitive-, and using the photon-stimulated desorption mode (PSD-NEXAFS), which is surface sensitive. By recording simultaneously those two signals, we have evidenced the differences between the surface and bulk electronic and atomic structures, for both amorphous porous ice condensed at 40 K and crystalline ice condensed at 150 K. We have also followed the bulk and surface evolutions of an amorphous ice film annealed from 38 to 147 K. A steep change in the local atomic structure of the bulk is observed, likely related to the high-density amorphous ice→low-density amorphous ice phase transition between 38 and 55 K. We have shown that the surface of crystalline ice is well ordered, but this order is different from that of the bulk. We have evidenced that the H_2O-H_2O intermolecular distance at the surface of ice is always longer than in the bulk, and that this difference increases with temperature, as the thermally induced reordering of the surface proceeds. SCF-Xα multiple scattering calculations allow us to figure out those structural differences, both in the bulk and at the surface of amorphous ice, but further calculations are necessary for crystalline ice. We have shown that the PSD-NEXAFS signal is sensitive to the surface morphology that changes with temperature because of the micropores collapse. We have used a model [E. Vichnevetski, A. D. Bass, and L. Sanche, J. Chem. Phys. **113**, 3874 (2000)] that quantitatively describes the effect of the surface porosity on the ion yield. The surface of ice at 38 K is well described by a network of vertical cylindrical pores of 20 Å of diameter, separated by 6 Å, collapsing when annealing the film. This model also properly accounts of the peculiar temperature evolution of the PSD signal at the $O1s^{-1}4a_1^{+1}$ excitation, and therefore, allows to establish the relation between the PSD-NEXAFS signal and the surface porosity. © *2002 American Institute of Physics.* [DOI: 10.1063/1.1519256]

I. INTRODUCTION

The study of the electronic and atomic structures of the surface of ice is of fundamental importance for the understanding of the physical and chemical properties of this material. In particular, one important domain where the surface of ice plays a key role is the heterogeneous chemistry of the earth stratosphere[1,2] and of the interstellar space.[3] On earth, the chemical reactions that come into play in the seasonal depletion of the stratospheric ozone take place at the surface of the polar stratospheric clouds that form when temperature drops during the winter. Those clouds are made of crystalline ice I_h, the phase naturally found on earth. Chlorinated molecules as $ClONO_2$, HOCl, HCl react after their condensation at the surface of these icy clouds, leading to the release of Cl_2 that destroys ozone after being dissociated by the solar radiation. In space, amorphous microporous ice is the most abundant form of water, and is believed to be at the heart of the thermally or photochemically driven reactions occurring between simple molecules as CO, NH_3, etc. condensed on/in ice, leading to the formation of more complex organic compounds as, e.g., amino acids.[4]

To understand at an atomic scale the first steps of these heterogeneous reactions, numerous spectroscopic and theoretical studies have attempted to probe or model the ice surface, bare or with molecules condensed on it. Among the experimental techniques that have been used, one can cite for instance the sum-frequency generation (SFG) for the study of the surface vibrational states. This technique gives accurate informations on the dangling OH bonds (which are the sites at which most of the reactions are supposed to occur[5]) and their orientations under various thermodynamical conditions, e.g., during the surface premelting.[6] Other vibrational probes as conventional Fourier-transform infrared (FTIR), when used under conditions for which the surface signal is enhanced compared to the bulk (grazing incidence,[7,8] microcrystalline deposits[5,9,10]), bring informations on the chemical form of the adsorbates at the surface and on the modifica-

[a]Author to whom correspondence should be addressed. Electronic mail: philippe.parent@lure.u-psud.fr

tions induced on the dangling OH bonds by the adsorbate. Structural techniques have also been used, for instance low energy electron diffraction (LEED),[11,12] helium atom scattering (HAS)[13] or glancing angle x-ray scattering (GAXS).[14] LEED combined with molecular-dynamic simulations has shown that an ice layer of at least 10 Å thick condensed at 140 K on Pt(111) is well ordered, and has a surface that is consistent with either the [0001] surface of bulk terminated hexagonal ice I_h or the [111] surface of cubic ice I_c.[12] This study has also shown that the first surface bilayer is disordered because of enhanced thermal motions. HAS performed on 100 Å thick ice films condensed at 150 K on Pt(111) also led to similar conclusions.[13]

At the side of those atomic-scale studies, the microscopic morphology of porous amorphous ice has also been extensively investigated. Porosity increases the surface area and the adsorption energy of the adsorbates,[15] and is therefore, a key parameter for the understanding of the reactivity of ice in astrophysical environments. N_2 adsorption isotherm,[15,16] temperature-programmed desorption,[5,17–20] optical or molecular beam interference measurements,[21,22] electron stimulated desorption[23–28] have been used for the determination of the surface area, the density, the size of the pores, the structure and the reactivity of the amorphous microporous ice.

Despite this tremendous amount of works (by far, not all of them are listed here), direct experimental informations on the atomic and the electronic structure of the surface layers of microporous or crystalline ices are still lacking. X-ray absorption spectroscopy (or NEXAFS for near-edge x-ray absorption fine structures) has been used since many years to study the structural and the electronic properties of crystalline or amorphous materials. It has been already employed for studying the bulk of ice at the O K-edge (530 eV).[29–32] However, the probed depth is too large (at least 50 Å) for surface studies. This technique is also insensitive to microscopic structures as pores (in amorphous microporous ice, typical size ~20 Å)[15] since the photoelectron is scattered within a volume that is smaller than 10 Å. Thus, if the NEXAFS spectroscopy allows to characterize the local atomic order, no informations on the microporous morphology of ice can be expected. Now, instead of measuring the x-ray absorption signal in the conventional manner (NEXAFS), that is—in the soft x-ray range—using the electron or the fluorescence yield, one can measure a minority channel, the ion photodesorption (PSD-NEXAFS for photon-stimulated desorption-NEXAFS).[29,33–37] In that case, the signal comes from the outermost molecular layers and thus provides structural and electronic informations on the ice surface, as normal NEXAFS does for the bulk. In addition, we will show that the ion photodesorption is also extremely sensitive to the microscopic roughness of the surface, since the outgoing ions can be scattered by the protrusions resulting from the open pores at the surface. Another general interest of this technique—which is not applied here but in other works we have performed[38,39]—is the use of the chemical selectivity of the x-ray absorption spectroscopy for studying the interaction of a foreign molecule with the ice surface. Indeed, PSD-NEXAFS recorded at the edge(s) of the contaminant will bring electronic and structural informations on the admolecules, and how they diffuse within the bulk. In addition, PSD-NEXAFS recorded at the O K-edge after the interaction allows to study the modifications induced in turn on the surface of ice.

In this paper, we present the NEXAFS and the PSD-NEXAFS results obtained on vapor-deposited ice films under UHV conditions, at 150 K where ice is crystalline and at 38 K where ice is porous and amorphous. In Sec. III A, we discuss the electronic spectra of the ice surface, the bulk of ice and the free H_2O molecule. In Sec. III B, we present the structural informations that can be deduced from the analysis of the continuum resonances. In particular, we show that the surface of ice is always less dense than the bulk, and that the surface of the crystal is quite well ordered. In Sec. III C, we present the evolutions with the temperature of the NEXAFS and the PSD-NEXAFS signals when annealing at 147 K an ice film deposited at 38 K. We observe a steep structural change in the bulk of amorphous ice between 38 and 55 K, assigned to the transition from the high-density form of amorphous ice $I_a h$ to the low-density form $I_a l$. The variations of the ion yield with the temperature show that the pores collapse when annealing the film. Those variations, both on the continuum and at the $4a_1$ excitations, allow to describe the morphology of the surface of the amorphous ice film thanks to the model of pores proposed by Vichnevetski *et al.*[27] We also show that this collapse is accompanied by a thermally induced surface relaxation, causing a continuous increase of the H_2O–H_2O distance at the surface.

II. EXPERIMENT

The experiments have been performed at LURE on the SuperACO storage ring (Orsay). The NEXAFS measurements have been done on the SA22 beamline equipped with a high-energy plane grating spherical mirror monochromator, with a resolution of ~100 meV at the O1*s* edge (530 eV). The energy of the monochromator was calibrated at the oxygen K-edge using the weak absorption feature due to the oxygen contamination of the optics. The measurements on the H_2O ice films have been done on the SACEMOR experiment (base pressure 1×10^{-10} Torr). The H_2O gas-phase spectrum was previously recorded in partial ion yield on the PAM6 experiment connected to the SA22 beamline, using the same energy resolution and the same energy calibration (within a margin error of 0.1 eV) than for the ice measurements. This calibration was set to match that of the H_2O gas-phase data published in Ref. 40 ($O1s\rightarrow4a_1$ resonance at 534 eV). On ice, the total electron yield (TEY) and the total ion yield (TIY) NEXAFS spectra have been collected simultaneously; they are, therefore, naturally calibrated one to the other. The TEY spectra are the ratio of the photocurrent of the sample on that of the beam monitor. The TIY measurements have been done using a 5 cm^2 two-stages microchannel plate (Galileo) positioned at 5 cm in front of the sample, and the TIY spectra are the ratio of the sample ion yield on the beam monitor photocurrent. The measurements have been performed at a grazing incidence of $10°\pm2°$ (the angle between the synchrotron beam and the surface). The microchannel plates were biased at −2.0 kV, the sample being

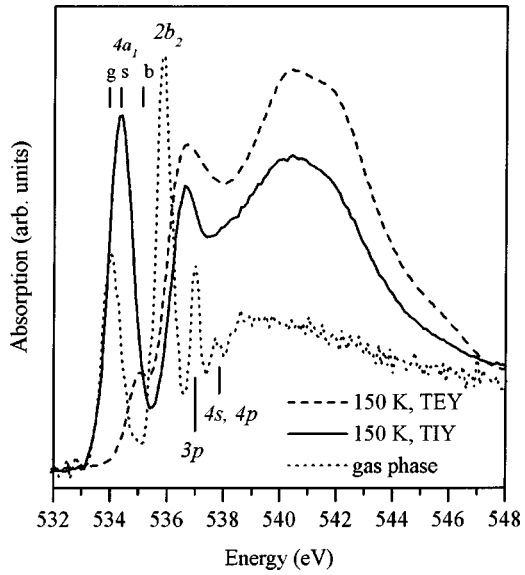

FIG. 1. O K-edge NEXAFS spectra of a 100 ML crystalline water ice film deposited at 150 K, recorded simultaneously in total electron yield (TEY, representative of the bulk) (dashed line) and total ion yield (TIY, representative of the surface) (solid line). The gas phase spectrum of water (dotted line) recorded on the same beamline is reported for comparison. Calibration between gas and solid spectra is within a margin error of 0.1 eV. The vertical ticks indicate the energy position of the $O1s \rightarrow 4a_1$ transition in the gas phase (g), at the surface (s), and for the bulk (b).

grounded; the resulting extraction field allows to detect all the desorbing cations, whatever is their emission angle relative to the surface normal. The ice films were deposited on a clean Au(111) single crystal mounted on a rotatable sample holder cooled by a temperature-controlled liquid helium cryostat. The temperature was measured by a platinum resistance welded to the substrate; temperature control and ramps were achieved by a feedback system driving the resistive heating of the helium bath. After the ultra pure H_2O was degassed by several freeze–pump–thaw cycles, thick ice films were prepared by dosing from the background 100 Langmuirs ($1L = 10^{-6}$ Torr.s) of H_2O vapor at a rate of 0.1 L.s^{-1} using a diffuser outlet located at the back of the substrate, in a special chamber isolated from the main analysis chamber to avoid further contamination during the recordings. Assuming a sticking coefficient of unity,[11,21] the estimated number of water layers deposited on the substrate is of 100 ML. In our dosing conditions, the ice films grown below ~120 K are amorphous and microporous; deposition above ~120 K generates nonporous amorphous ice films. This form is metastable and transforms into crystalline ice above 150 K, in the hexagonal form I_h or in the cubic form I_c.[11] The two forms only differ in the stacking sequence of the water bilayers, and so, starting from a central oxygen atom, the two first molecular coordination shells are the same in ice I_h and in ice I_c. They are thus hardly distinguishable with the NEXAFS technique, and we will label those films simply as ''crystalline.''

III. RESULTS AND DISCUSSION

A. Bulk and surface electronic structures

The Fig. 1 presents the TEY and TIY spectra of a 100 ML crystalline H_2O ice film deposited at 150 K in the near-edge region (532–548 eV); they are compared to the gas-phase spectrum of H_2O. The TEY spectrum is representative of the bulk of the film, because of the large escape depth of the Auger/secondary electrons (~50 Å). On the contrary, photo-ions have a very low kinetic energy, and the fragments emitted from the bulk are readily stopped by inelastic collisions. Only the ions emitted at the very surface are able to escape, and the TIY signal is thus representative of the outermost layer of the condensed film.[29]

On the gas-phase H_2O spectrum, the first two sharp resonances are attributed to the $O1s \rightarrow 4a_1$ transition (534 eV, Γ(FWHM) = 0.78 eV) and to the $O1s \rightarrow 2b_2$ transition (535.9 eV, $\Gamma = 0.62$ eV). Then follow transitions to pure Rydberg states $O1s \rightarrow 3p(b_1)$, $3p(a_1)$ (537 eV) and $O1s \rightarrow 4s$, $4p(b_2)$, $4p(b_1)$, $4p(a_1)$ (537.8 eV).[40,41] On the TEY spectrum, the shoulder at 535 eV is assigned to the $O1s \rightarrow 4a_1$ transition, shifted by +1.0 eV and broadened ($\Gamma = 0.98$ eV) compared to the gas phase. This upward shift indicates that the $4a_1$ state becomes more antibonding upon condensation, a result of an increase in the bonding character of the valence states caused by the hydrogen bonding between the water molecules.[33] On the TIY spectrum, the $O1s \rightarrow 4a_1$ transition is located at 534.3 eV, between the gas-phase value (534 eV) and the TEY value (535 eV). Its linewidth (0.98 eV) is broader than for H_2O gas (0.78 eV) and is equal to the TEY value. Its intensity is strongly enhanced with respect to the continuum region: It is 6 times higher than on the TEY measurement. Above the $4a_1$ resonance follows a quite narrow resonance located at the same value than on the TEY spectrum (536.5 eV). It could be a remain of the $2b_2$ transition observed in the free molecule at 535.9 eV; this state being nondissociative,[42] no resonant fragmentation (no ion yield enhancement) is expected at this excitation.[43] The $3p$ and the $(4s,4p)$ Rydberg states strongly overlap the surrounding molecules [for instance, the $3p(b_1)$ orbital radius ($\langle r^2 \rangle^{1/2} = 3.65$ Å) is well larger than the O–O distance in between two water molecules (2.76 Å)],[29] and they are no longer distinguishable in ice as molecular states.

Mass filtered H^+ yield data published to date with a photon resolution similar to our measurements,[34] or with lower resolutions,[29,33,44] show the same trends than the TIY experiment presented here. This results from the fact that the H^+ ions are by far the most abundant species compared to other fragments, as OH^+, O^+, etc. Indeed, we did not detect other ions than H^+ using our quadrupole mass spectrometer. Coulman *et al.* have also reported that the H^+ ion yield at 530–540 eV is about 1000 times higher than the other ion yields.[33] Thanks to their low mass, only H^+ readily desorbs so that the H^+ yield strongly dominates the total ion yield signal.[45] Thus, we assume that our TIY data can be interpreted as a *mass filtered* photodesorption experiment measured through the H^+ yield.

The enhanced H^+ emission at the $O1s \rightarrow 4a_1$ excitation is due to the fact that the breakage of the OH bond is more efficient at this resonance than on others.[43] This bond breaking has been suggested to take place *before* the core hole

decay (ultrafast dissociation, or UFD)[33–37] thanks to the steepness and to the repulsive nature of the potential energy surface of the $O1s^{-1}4a_1^{+1}$ final state in the Franck–Condon region.[40,46] In the gas phase, partial ion yield and resonant Auger experiments at the O K-edge also support this hypothesis.[47] For ice, the situation is actually less clear. UFD should lead to desorption of neutral H^0 fragments, so far not detected by Romberg *et al.*[34] at the $O1s \rightarrow 4a_1$ *surface* excitation (albeit well detected for the *bulk* $4a_1$ excitation). These authors assume that the neutral H^0 particles coming from the UFD channel are ionized by transferring one electron to the matrix before leaving the surface (thus, unexpectedly, for condensed H_2O, the UFD channel will enhances the H^+ emission at the $4a_1$ excitation). At the side of the UFD process, fragmentation also occurs *after* the core hole decay: The normal decay routes will also efficiently contribute to the H^+ yield, as for instance in the $1b_1^{-1}3a_1^{-1}4a_1^1$ and $1b_1^{-2}4a_1^1$ states, known to produce H^+ emission at the $4a_1$ state excitation in ice.[41]

The enhancement of the $4a_1$ transition is strongly maximized when the electric field ϵ of the synchrotron beam is directed along the surface normal **n** of the ice film, as reported in detail by Coulman *et al.* in Ref. 33. Our experiments have also been done in such grazing geometry $[(\epsilon,\mathbf{n})=10°]$, with the detection direction essentially normal to the surface. Coulman has suggested that this polarization dependence is related to a preferred orientation of the molecules at the surface, and that the peaking of the H^+ signal around the surface normal is due to the breaking of the molecules having one of their OH bond oriented along **n**. The molecules in this configuration are those with one of the OH bond participating to the hydrogen bonding with the neighboring molecules and keeping the other OH bond free, sticked up out the surface and directed toward the vacuum. This former bond is usually called the «dangling» OH bond (noted d_{OH}).[48] In the idealized hexagonal $I_h[0001]$ ice surface (and also at the $I_c[111]$ surface), a third of the sites are occupied by those d_{OH} molecules, an other third by three-coordinated dangling O molecules (those having their two OH groups hydrogen bonded with two other molecules, noted d_O), and the last third by normal four-coordinated molecules located at the bottom of the ice bilayer (noted s-4). Those two latter configurations are not expected to contribute a lot to the enhancement of the ion yield at the $4a_1$ transition, since the OH bonds of these molecules are not oriented along **n**. Indeed, when fragmentation occurs at the d_O or s-4 sites, the escape probability of the H^+ fragment is likely weak, since the OH axis are directed toward the bulk or at most parallel to the surface, and not toward the vacuum as for the d_{OH} molecules. We, therefore, assume that the fragmentation of the dangling OH bond is the dominant contributor to the enhanced ion yield at the $4a_1$ resonance, which can be thus considered as a fingerprint of the d_{OH} molecules. The -0.7 eV energy shift of the $4a_1$ resonance on the TIY spectrum compared to the TEY (Fig. 1) then mostly reflects the differences in the electronic structure of the surface d_{OH} molecules compared to the bulk molecules. It is noteworthy that the $4a_1$ state of the d_{OH} molecules is close ($+0.3$ eV) to the gas-phase value, indicating that they own an electronic configuration close to the free molecule, less antibonding than in the solid, as expected since one hydrogen bond is missing. However, the linewidth of the surface $4a_1$ state is the same than in the bulk (0.98 eV) and is broader than in the gas phase (0.78 eV), indicating that solid state effects modify the shape of the potential energy surface of the $O1s^{-1}4a_1^{+1}$ state even at the d_{OH} sites.

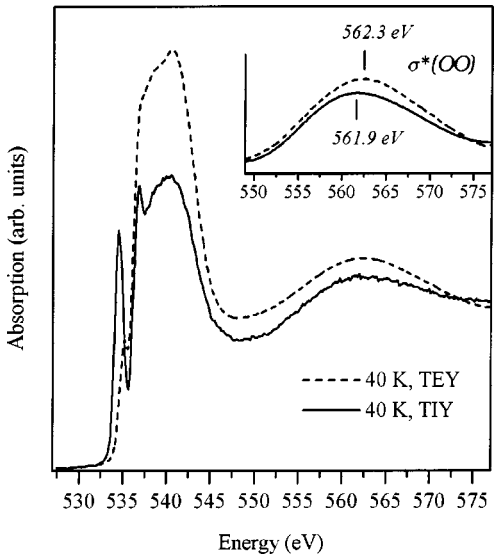

FIG. 2. TEY (dashed line) and TIY (solid line) spectra of a 100 ML amorphous ice film deposited at 40 K. On the inset are compared the corresponding σ^*(OO) resonances (see text), background-substracted and smoothed for display (TEY: dashed line; TIY: solid line).

B. Bulk and surface atomic structures

On the Fig. 2 are compared the TEY and TIY NEXAFS spectra of a 100 ML porous amorphous ice film deposited at 40 K. The spectra have been normalized to 1 at 573 eV for display. The broad resonance located at 562.3 and 561.9 eV on the TEY and the TIY spectra, respectively (see the inset on the Fig. 2), is not present in the gas phase, and results from the scattering of the photoelectron between the neighboring water molecules. We call this resonance σ^*(OO); this is the first EXAFS oscillation.

To derive structural informations from this resonance, one important question is whether the ion yield in this energy domain is due to the fragmentation of the *surface* molecules after their own photoexcitation (''PSD,'' for photon stimulated desorption), or if it is due to the fragmentation of the surface molecules caused by the Auger and secondary electrons emitted by the molecules photoexcited *in the bulk* (''XESD,'' for X-ray induced electron stimulated desorption).[49] In the XESD mechanism, the electrons emitted from the bulk can induce nonresonant fragmentation of the surface molecules by, e.g., interband transition, dissociative electron attachment, etc. In that case, the fragmentation is simply proportional to the electron yield, and the ions emitted through XESD will give a signal similar to the TEY. PSD results from the fragmentation of the surface molecules after their own core excitation, and this gives rise to a spectrum strongly different from the TEY, bringing informations

on the electronic state and on the structure of the surface. Since the TIY signal in the continuum part of the ice spectrum *is not similar* to the TEY, we conclude that in the case of our experiments, the PSD mechanism dominates the XESD. Thus, we can safely derive structural informations about the surface layer from our ion yield measurements.

The scattering theory predicts that the $\sigma^*(\mathrm{OO})$ resonance energy is proportional to $1/R^2$, where R is the distance between the O–O atoms in the first coordination shell.[50] Therefore, the longer is the O–O distance, the lower is the $\sigma^*(\mathrm{OO})$ energy. The -0.4 eV shift of the $\sigma^*(\mathrm{OO})$ resonance in the TIY signal compared to the TEY signal indicates that the mean O–O distance at the surface is longer than in the bulk. Contrary to the case of the $4a_1$ excitation, which is an intramolecular level, the ions emitted at the $\sigma^*(\mathrm{OO})$ result from the Auger decay of the $\mathrm{O}1s^{-1}\sigma^*(\mathrm{OO})^{+1}$ state, thus involving a resonant intermolecular scattering state. This resonance is not only due to the scattering of the photoelectron by the surface molecules, but also, in principle, by those directly underneath. Therefore, the ions emitted at this resonance actually hold structural information that also comes from the layers underlying the surface. Let us call that probed depth «the near surface». This depth is related to the space where coherent scattering of the photoelectron can occur; this is the volume around the absorbing atom where a certain structural order exists. Note however that this volume is intrinsically limited in size by the photoelectron mean free path, that is typically less than 10 Å for photoelectrons of about 30 eV of kinetic energy[51] [at the maximum of the $\sigma^*(\mathrm{OO})$ resonance, the kinetic energy of the photoelectron is 26 eV, taking the ionization threshold as the inflexion point of the experimental data (536 eV)]. In the case of amorphous ice, the structural ordering only exists within the first molecular coordination shell, that is ~3 Å, and no coherent scattering can occur beyond. Taking the ice $I_h[0001]$ as a model surface, such probed depth of 3 Å from the surface will include the second bilayer. However, for a d_{OH} molecule photoexcited at the surface, the only neighbors located within 3 Å are in the plane of the top bilayer and not in the underlying one. Thus, the $\sigma^*(\mathrm{OO})$ resonance results from scattering events occurring only within the outermost bilayer. To estimate the lengthening of the intermolecular distances within the first molecular coordination shell, we have performed SCF-Xα multiple scattering (MS) calculations using the FEFF-8 code[52] on a cluster of five H_2O molecules tetrahedrally arranged as in ice I_h.[53] As expected for amorphous ice, such cluster was sufficient to model the $\sigma^*(\mathrm{OO})$ resonance. The calculated spectrum shows a broad resonance centered at 561.1 eV (exp. value 562.3 eV), mainly coming from the single scattering with the surrounding oxygen atoms in the tetrahedron. Then, we have lengthened the O–O distance in order to obtain a downward shift of the $\sigma^*(\mathrm{OO})$ of -0.4 eV in the calculation. Taking $d(\mathrm{O–O}) = 2.76$ Å,[54] we have found that the -0.4 eV shift corresponds to a lengthening of 0.010(5) Å of the O–O distance. Thus, we conclude from those calculations that, for amorphous ice at 40 K, the average density within the first surface bilayer is lower than in the bulk, the mean H_2O–H_2O intermolecular separation being of 2.77 Å instead of 2.76 Å (bulk value). Recently, a study comparing the TEY and TIY EXAFS data on liquid water[55] has also evidenced a strong lengthening of the O–O distance at the surface of water compared to the bulk (3.00 Å vs 2.85 Å), lengthening which is dramatically larger than what we observe between the surface and the bulk of amorphous ice (2.77 Å vs 2.76 Å). These figures reflect the fact that the hydrogen bonding at the surface of water is considerably weaker than at the surface of ice, itself weaker than in the bulk.

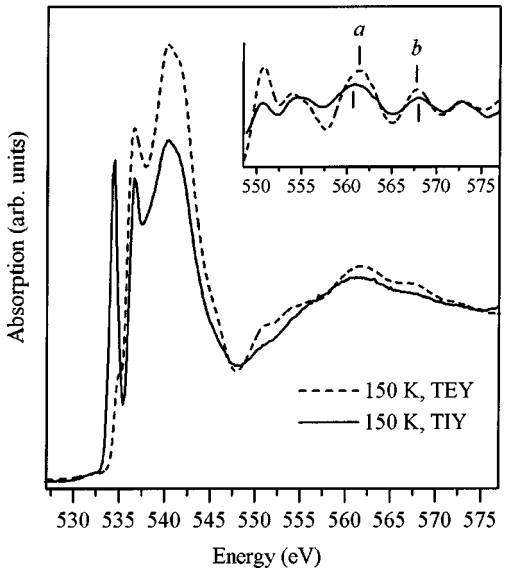

FIG. 3. TEY (dashed line) and TIY (solid line) spectra of a 100 ML crystalline ice film deposited at 150 K. On the inset are compared the multiple scattering (MS) resonances observed on these spectra, substracted from the broad $\sigma^*(\mathrm{OO})$ resonance contribution and smoothed for display. The vertical ticks are guide to the eyes for the energy shifts between bulk (TEY, dashed line) and surface (TIY, solid line) contributions of the MS resonances labeled *a* and *b*.

Figure 3 presents the TEY and the TIY NEXAFS spectra of a crystalline ice film deposited at 150 K. We observe wiggles superimposed to the $\sigma^*(\mathrm{OO})$ resonance, which are absent in the amorphous phase. This time, they result from the coherent multiple scattering of the photoelectron within the second and next molecular shells, because of the existence of a long-range order in crystalline ice. A single molecular shell cluster is therefore not sufficient to model these MS structures, and a larger cluster including the second and next ordered shells is necessary. Indeed, in the case of crystalline ice, coherent scattering can occur in a larger volume than in amorphous ice, but not beyond 10 Å, as said above. Starting from an absorbing molecule at the surface, a probed depth of 10 Å corresponds now to about three molecular bilayers. So far, our SCF-MS-Xα calculations performed on a cluster made by three bilayers did not allow a satisfactory agreement with the observed MS features. It could be that the hydrogen contribution is important in the scattering process,[30] and such calculations including hydrogen are to date very difficult to perform due to the muffin tin potential approximation.[32] Qualitative information can be, however, obtained from the comparison between TIY and TEY. The inset of the Fig. 3 shows the MS part extracted from the NEXAFS signal for the TEY and TIY signals. One can see

that the MS structures present on the bulk spectrum are still observable on the TIY signal, damped in intensity, and with significant energy shifts. For instance, the resonance labeled *a* located at 561.4 eV on the TEY signal is strongly shifted downwards (−0.6 eV) on the TIY signal (560.8 eV). On the contrary, the resonance *b* is a bit shifted upwards (+0.2 eV) (568.2 eV on the TIY, 568.0 eV on the TEY signal). The observation of the MS features on the TIY signal clearly indicates that the surface of the crystalline ice film remains well ordered, within the three outermost bilayers. The energy shifts observed on the TIY MS features indicate that the mean positions of the molecules within these three bilayers are different from those of the bulk, likely because of the surface relaxation. The damping of the MS amplitude of the TIY signal can originates from an enhanced thermal motion of the molecules at the surface of the crystal[11,13] resulting from the weakening of the hydrogen bonding between the water molecules at the surface, and also from the fact that the number of MS pathways is reduced, since the scattering processes from the excited surface molecules occur only in a half-space compared to the scattering in the bulk.

Beyond these qualitative informations, we expect from further SCF-MS Xα calculations a better agreement with the TEY experimental signal, so that it will be possible to obtain the accurate positions of the water molecules far around a central absorbing O atom, and thus it could become possible—albeit difficult—to distinguish between the I_h and I_c forms of crystalline ice (differences can be found in the third molecular shell around the absorbing molecule). In addition, an accurate calculation of the MS part of the TIY signal will give access to the crystallographic order within the three first bilayers of the ice surface, an experimental key test of the computational simulations of the ice surface, which are very useful for the understanding of the physical and chemical properties of ice.

C. Evolution with temperature

1. Bulk signal

Figure 4 presents the evolution of the TEY spectra of a porous amorphous H_2O film deposited at 38 K and heated up to 147 K (2 K/min; at each temperature step, the sample temperature is stabilized during the acquisition time, which is of about 30 min). A further annealing at 160 K led to crystallization; at this temperature the film starts to get thinner, and desorption is completed at 170 K. The maximum of the σ^*(OO) resonance located at 562.3 eV at 38 K steeply changes to 562.7 eV at 55 K, and then remains constant from 55 to 147 K. This corresponds to a slight shortening of the *bulk* O–O distance of about 0.010(5) Å between 38 and 55 K. Structural evolutions in this temperature range on vapor deposited amorphous ice films under vacuum conditions have been studied by x-ray diffraction by Narten *et al.*,[54] and also by electron diffraction by Jenniskens *et al.*[4] These studies have both shown that the amorphous films deposited at low temperature (10–15 K) have a specific high-density structure at the atomic scale («ice $I_a h$») that persists until about 38 K, and then undergoes a well defined transition to a low-density amorphous form at higher temperatures

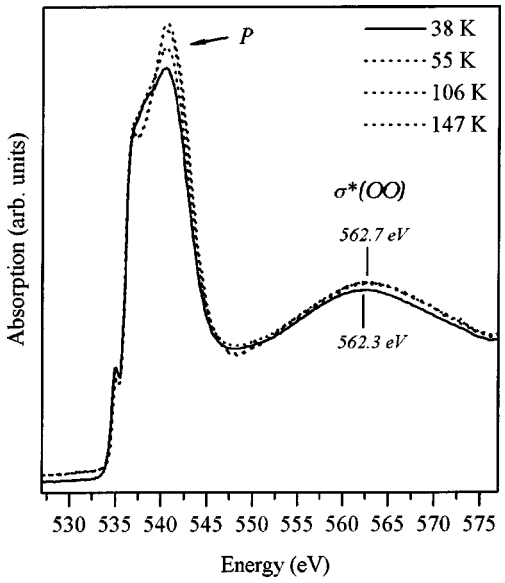

FIG. 4. Evolution with temperature (38–147 K) of the TEY spectra (raw data) of an amorphous ice film deposited at 38 K. The spectrum at 38 K (solid line) has been slightly down shifted vertically for display. Note the steep change in the σ^*(OO) resonance energy between 38 K (562.3 eV) and the higher temperatures (562.7 eV for $T \geqslant 55$ K). The spectra recorded at 55, 106, and 147 K have not been shifted for presentation; the intensity of the resonance labeled *P* on the figure increases with temperature, and thus allows to make the distinction between the 55, 106, and 147 K data in this energy domain.

(«ice $I_a l$»). Narten *et al.* have shown that the high-density of the ice $I_a h$ results from the presence of ~1.4 additional water molecule in average, located in interstitial position (at 3.3 Å from the central water molecule) inside an amorphous network of tetrahedrally coordinated water molecules, with about 8° of angular distortion from the normal tetrahedral value. This study has also shown that the main O–O separation in ice $I_a h$ is 2.76(1) Å, the same than in ice $I_a l$, but with a wider O–O distance dispersion. In our work, the decrease in the O–O distance observed when annealing the ice film from 38 to 55 K is likely related to the $I_a h \rightarrow I_a l$ structural transition described by Narten and by Jenniskens. However, as said, no change in the O–O distance within the first coordination shell was reported in their works. The slight contraction [0.010(5) Å] of the first molecular shell deduced from our data is actually within the margin error of the O–O distance calculated by Narten *et al.*, and thus can have been missed in their experiment. The presence of interstitial H_2O molecules in the $I_a h$ form is a possible reason for the larger intermolecular distance observed at 38 K. It could be related to the perturbation of the angular correlation in the structure of the amorphous ice deduced from the diffraction data of Narten, and we suggest that this could change the intermolecular distances as well. Last, we do not observe much changes in the spectra for $T > 55$ K, except in the 536–544 eV energy domain, where variations in shape are observed (see the resonance *P* on the Fig. 4). This results in the evolution of the band structure of the amorphous solid with temperature, likely related to the narrowing of the angular dis-

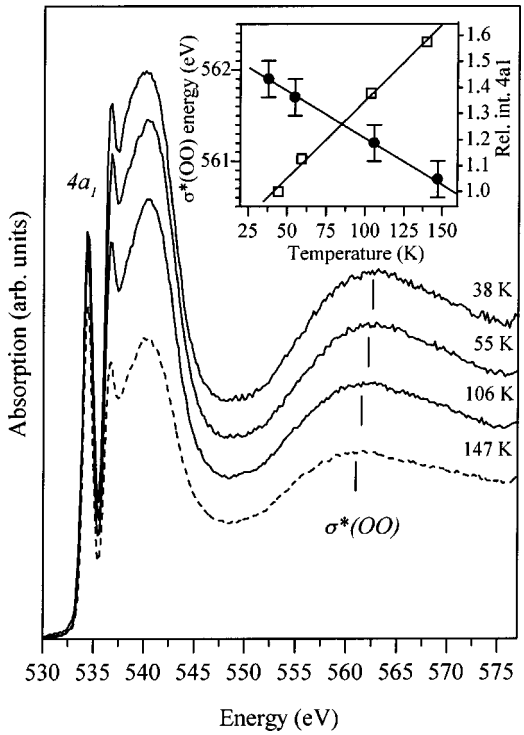

FIG. 5. Evolution with the temperature (38–147 K) of the TIY spectra (raw data) of an amorphous ice film deposited at 38 K, recorded simultaneously with the TEY data presented Fig. 4. Note the continuous decrease of the ion yield in the continuum energy domain (above 536 eV), whereas the $4a_1$ intensity remains almost constant between 38 and 106 K, and then decreases at 147 K (dashed line). On the inset is reported the evolution with temperature of the $4a_1$ intensity relative to the integrated ion yield (526–582 eV) divided by its value at 38 K (open squares, right axis). On this inset is also shown the shift with temperature of the σ^*(OO) resonance energy (filled circles, left axis).

persion of the tetrahedral angles between molecules with temperature, a result of the increasing ordering of the ice lattice.

2. Surface signal

Figure 5 presents the raw TIY spectra corresponding to the TEY data shown on the Fig. 4 (i.e., the TEY and the TIY signals have been recorded at the same time, for each temperature step). When the film is heated, one observes: (1) A strong decrease of the ion yield intensity in the continuum (above 536 eV); (2) with respect to the continuum part of the spectra, the intensity of the $4a_1$ resonance increases; (3) the σ^*(OO) resonance shifts from 561.9 eV at 38 K to 560.8 eV at 147 K. In the following, we discuss each of these three points:

(1) Although the integrated TEY signal remains almost constant in intensity when the temperature increases (Fig. 4), the ion emission (integrated from 536 to 582 eV) is reduced of a factor of 2 from 38 to 147 K. As already said, amorphous ice films deposited below ~120 K under ultrahigh vacuum conditions are porous at a nanoscopic scale, with pores of a typical dimension of some tens Å.[15] A sintering of the microporous ice at temperatures above 130 K leads to nonporous amorphous films; finally, around 150 K, ice becomes crystalline. The preparation conditions are known to greatly influence the structural forms and the specific surface areas of those films, indicating that the energy differences between these different forms/morphologies are faint. It has been shown in particular by Stevenson *et al.*[16] that the angular distribution of the incident water molecules during the deposition of the film is as important as the temperature in determining the morphology of the microporous ice film. By varying the angle of the water beam impinging a cold substrate, they have shown that porosity is almost inexistent when the water beam is directed normal to the surface. At 60°, porosity becomes as high as for films background deposited (as those studied here), where it is maximum.

The effects of the porosity of ice on ion desorption have been studied on the electron-stimulated desorption (ESD) of D^+,[23,24,56] D^-,[25] and O^- from O_2 condensed on D_2O ice films.[26] In this latter work, it has been shown that the O^- ESD yield from 0.3 ML of O_2 condensed at 15 K on 8 ML of D_2O strongly increases as the growing temperature of the ice films is increased from 15 to 150 K. This arises from the fact that the number and the size of the pores are reduced with increasing the temperature. For the same amount of adsorbed oxygen on the film, the quantity of O_2 at the surface decreases when porosity increases. The O^- ions emitted from O_2 molecules adsorbed deep in the pores can not desorb due to collisional effects within the pores channels, reducing their kinetic energy, thus their escape probability. Sieger *et al.*[23,24] have also made this assumption to interpret the increase of the ESD D^+ yield from ice films deposited at 90 K, then annealed at 130 K to block up the pores and cooled at 90 K: The D^+ yield is about 40% higher after the pores collapse than before.

In our experiments, we observe the *opposite* effect: The ion yield decreases during the sintering of the film. As pointed out by Sieger,[23] porosity brings two competitive effects: The presence of pores increases the surface area, thus the number of sites at which ions can be emitted (''source effect''), but pores also play the role of an ion sink, because of the signal attenuation resulting from the interaction of the outgoing ions with the pores walls (''sink effect''). In our experiments, and contrary to those cited above, the source effect clearly dominates the sink effect. It can be that our films have a different morphology: In the D^+ experiment reported in Refs. 23 and 24, the films are grown at 90 K, whereas our deposition temperature is 38 K, thus our films are likely more porous. In the O_2 experiment reported by Azria *et al.* in Ref. 26, the films were grown with dosing from a nozzle located at 85° from the surface normal, that can also change their morphology compared to background deposited films: In the experiments reported by Stevenson,[16] the quantity of adsorbed N_2 on ice films deposited at 85° is reduced by about 30% compared to background deposited H_2O. Finally, the PSD processes also result from excited states that are different than in ESD. For instance, the D^+ emission from low energy electron impact mainly arises from 2h1e excitations (the dominant channels are $3a_1^{-1}1b_1^{-1}4a^{+1}$, $1b_1^{-2}4a_1^{+1}$ and $3a_1^{-2}4a_1^{+1}$),[56] whereas in

our PSD experiment, the essential of the integrated ion yield we discuss here arises from $2h$ normal Auger decay states. The ions emitted from those states can have a higher kinetic energy[56] and/or different angular distribution than the $2h1e$ excitations, so their sensitivity to collisional effects may be different. In addition, the linear polarization of the synchrotron light, the detection geometry and the different penetration depths between x-ray photons and low energy electrons can also lead to different results.

The gain in surface area due to porosity and being still efficient for particle desorption has been estimated by Vichnevetski *et al.*[27] in their N_2^* ESD study from N_2 adsorbed at 20 K on ice films grown microporous amorphous (20 K) or crystalline (150 K) for various dosings of N_2. In line with the experiments reported by Azria *et al.*, they have observed that on a thick microporous film deposited at 20 K, the amount of N_2 necessary to obtain the same rate of N_2^* species than on a crystalline film deposited at 150 K is systematically larger. They have proposed a geometrical model of pores accounting well for their data. It consists in a regular hexagonal arrangement of cylindrical pores parallel to the surface normal of the film. Particles emitted from the surface of the pores deep within the film cannot escape due to collisions/de-excitations, and only the ions located near the film–vacuum interface can desorb. Assuming that this effective escape depth b is proportional to the pore radius r, i.e., $b=k.r$ where k is the constant of proportionality, the area A_d of the film from which desorption may occur is given by[27]

$$A_d=\frac{A}{3}\frac{(3a^2-2\sqrt{3}\pi r^2+4\sqrt{3}\pi kr^2)}{a^2},$$

where a is the distance between the center of the pores and A is the surface of a nonporous film. We now apply this model to our experimental results, making the reasonable assumption that there is no polarization dependence of the PSD yield in the continuum of state. Taking $A_d=2\,\mathrm{A}$, since the ion yield at 38 K is two times higher than at 147 K (assuming the film ideally flat at this temperature), and taking $r=10$ Å and $a=26$ Å from Vichnevetski, we find an escape depth $b=14$ Å, close to the value of 11 Å they have obtained. Thus, the surface of the film at 38 K is well simulated by a surface riddled by large vertical cylindrical pores of 20 Å of diameter separated by 6 Å. Thus, about 57% of the surface of the film is pierced by pores, showing that the roughness of our microporous ice films deposited at 38 K is quite high. In reality, the pores are irregular in shape, interconnected and of a complex geometry, and this model is a simple approximation.

In our experiment, we must also take account of the intrinsic variation of the ion yield with the temperature. On ice, this effect has been studied in detail by Sieger *et al.*[56] They have shown that the D^+ ESD yield from D_2O ice increases between 135 and 160 K for a crystalline film deposited at 155 K, a result of the enhanced molecular character of the surface molecules when annealing. Temperature weakens the hydrogen bond lattice, changing the lifetime of the a_1 excited valence levels, increasing the D^+ yield. By enhancing the ion emission, this effect could then reduce the decrease in the PSD yield due to the pores collapse, mainly when the temperature approaches 147 K. To measure the intrinsic temperature dependence of the ion emission, we have cooled at 38 K a crystalline ice film deposited at 150 K (not shown here), where there is no possible morphological changes. No significant variations in the ion yield have been detected on the whole TIY spectrum, from 150 to 38 K. Thus, we conclude that the intrinsic temperature effect is negligible on the PSD yield. Therefore, the variations of the ion emission observed when annealing a porous ice film are only dominated by the pores collapse.

(2) The second fact that stems from the results presented Fig. 5 is the relative increase of the ion emission at the $4a_1$ resonance with respect to the rest of the spectrum. For each temperature, doing the ratio between the maximum of the $4a_1$ state with the integral of the ion yield between 536 and 582 eV (and expressing this ratio as a percentage of its value at 38 K), we observe that the relative increase of the ion yield at the $4a_1$ excitation is almost linear and, at 147 K, is 57% higher than the value at 38 K (see the inset on the Fig. 5).

Previously, we have seen that the collapse of the pores reduces the number of ion emitters, so the signal in the continuum of state decreases with the temperature. This must be also the case for the $4a_1$ excitation, but since its relative intensity increases, it is clear that the ion emission at this state becomes more efficient when the pores collapse. As said Sec. III A, the $4a_1$ peak is built on the resonant fragmentation of the OH bond of the molecules being in a dangling OH site and having the OH axis oriented parallel to the electric field of the beam $\boldsymbol{\epsilon}$.[33] In addition, the $4a_1$ intensity is maximized when the OH bonds are oriented normal to the substrate, which is the case for the areas of the ice film which are flat and parallel to the substrate. Conversely, the intensity of the $4a_1$ strongly decreases when the OH bonds are oriented perpendicular to $\boldsymbol{\epsilon}$. Thus, the ion yield at the $4a_1$ excitation is enhanced when the dangling OH are directed at the same time along the surface normal and along $\boldsymbol{\epsilon}$. Starting from a very perturbed morphology at low temperature, the annealing has produced a smoother film, that is to say that the area oriented parallel to the substrate has certainly increased with the temperature. Thus, the number of dangling OH oriented both parallel to $\boldsymbol{\epsilon}$ and parallel to the surface normal $\mathbf{n}$ must have increased. Let us return to the model of porous surface proposed by Vichnevetski. At the grazing incidence, the normal $\mathbf{n}$ of the top of the film is oriented almost along $[(\boldsymbol{\epsilon},\mathbf{n})=10°]$, whereas the normal of the walls of the vertical cylindrical pores are almost perpendicular to $\boldsymbol{\epsilon}$. We can thus assume that the ions emitted at the walls of the pores only weakly contribute to the $4a_1$ resonance. In this model, when the pores are blocked up, the gain in surface area oriented parallel to the substrate is simply the area of the top of the pores (not that of the walls), that is the area of a circle πr^2 (r is the pore radius). Let us call $S_{\parallel}$ the portion of the surface parallel to the substrate; the gain in the $4a_1$ intensity must be equal to the gain in $S_{\parallel}$, since the molecules having their OH dangling bonds oriented parallel to $\mathbf{n}$ can only be found at this surface. In this model, before the pores collapse, we have $S_{\parallel}=a^2\cos 30°-\pi r^2$ (a is the pores separation); after the collapse, we have $S_{\parallel}=a^2\cos 30°$. Taking

again $a=26$ Å and $r=10$ Å, the gain in $S_{\parallel}$ is of 46%. Thus, the increase of 57% in the ion emission at the $4a_1$ is in satisfactory agreement with the gain in $S_{\parallel}$ resulting from the pore collapse. The slight discrepancy with the model (46% vs 57%) could come either from the choice in the initial set of the geometrical parameters r and a, or from the fact that the emission at the walls of the pores contributes a bit to the $4a_1$ intensity. This reflects the fact that the model proposed is a simple vision of the surface: In average, the pores are certainly not perpendicular to the substrate, but are oriented in a random manner, and a (small) portion of these pores can have a direction allowing an efficient emission at the $4a_1$ state from their walls.

(3) As discussed in Sec. III C, there is no measurable change in the intermolecular O–O distance in the bulk of ice from 55 to 147 K. Conversely, at the surface, we observe an important and linear decrease of the $\sigma^*(\mathrm{OO})$ resonance position, from 561.9 eV at 38 K to 560.8 eV at 147 K (see the inset on the Fig. 5). From the SCF-Xα MS calculations we have performed on a single-shell molecular cluster, this corresponds to an increase of about 0.030 ($\pm$0.015) Å in the H_2O–H_2O distance at the surface when annealing from 38 to 147 K. Thus, starting from the value of 2.77 Å at 38 K (see Sec. III B), the average intermolecular distance at the surface of ice lengthens continuously up to 2.80 Å at 147 K, probably because of the elongation of the hydrogen bond. At low temperature, the molecules impinging the ice film have insufficient translational energy to rearrange before being buried by subsequent adsorption: This causes the formation of the pores.[57] An increase in the film temperature activates the molecular motions, and a well-known consequence is the collapse of the pores and a decrease in surface area. In addition, at about 160 K, amorphous ice crystallizes. Therefore, these molecular motions lead not only to morphological changes at large scale (the pores), but also at the molecular scale since the structural ordering increases with the temperature. This is precisely what we observe here, and the new experimental observation that stems from our data with respect to this point is that at the surface, the morphological changes go with a surface reorganization at the molecular scale that proceeds through a lengthening of the H_2O–H_2O intermolecular distance, from 2.77 to 2.80 Å between 38 and 147 K.

IV. CONCLUSION

(i) We have compared the O K-edge TEY and TIY NEXAFS spectra of a crystalline ice film with the gas-phase NEXAFS spectrum of water, being calibrated within a margin of error of 0.1 eV. To our knowledge, it is the first time that this comparison is done with the same energy scale (and resolution), giving the accurate experimental energy shifts from gas→surface →bulk, specially for the $4a_1$ transition.

(ii) We have shown that in the case of ice, and in the conditions of our experiments, the PSD process dominates the XESD mechanism, and thus structural informations about the ice surface can be obtained from the scattering resonances measured in TIY.

(iii) From the energy shifts of these resonances between the TEY and TIY data, we have figured out the differences in the H_2O–H_2O distances between the surface and the bulk of ice at 38 K (2.77 Å instead of 2.76 Å for the bulk), thanks to the SCF-Xα multiple scattering calculations we have performed.

(iv) When deposited at 150 K, the TEY and TIY spectra indicate that ice is crystalline both in the bulk and at the surface. The mean crystallographic positions of the molecules in the three first bilayers are however different than from the bulk. Further SCF-Xα multiple scattering calculations of the TEY and TIY spectra of crystalline ice will allow to simulate both the bulk structure (distinction between ice I_c or ice I_h could then be made) and the surface.

(v) We have deduced from the evolution of the TEY spectra between 38 and 147 K that at 38 K, the bulk has the high-density form $I_a h$ of the amorphous ice. When heated at 55 K, a steep phase transition to the normal low-density form $I_a l$ is observed. The H_2O–H_2O bulk distances slightly decrease (-0.01 Å) because of this structural transition. From 55 to 147 K, no further change in the bulk intermolecular distance has been observed.

(vi) We have used a model of pores that well accounts for both the decrease of the ion yield in the continuum of state and its increase at the $\mathrm{O}1s^{-1}4a_1^{+1}$ excitation with temperature. The decrease of the PSD signal in the continuum of state indicates that the surface of the microporous ice film at 38 K is quite well approximated by a dense network of vertical pores of 20 Å of diameter, separated by 6 Å, from which only the ions emitted at their walls down to 14 Å from the surface are able to escape in the vacuum. When annealing, the pores are blocked up, the surface becomes smoother and as a result, the number of OH bonds properly oriented for an efficient ion emission at the $\mathrm{O}1s^{-1}4a_1^{+1}$ excitation increases. This increase is in good agreement with the gain in $S_{\parallel}$ calculated from the model, indicating that most of the molecules at the walls of the pores do not contribute to the ion yield at this state, a result of the strong polarization dependence of the PSD process at the $4a_1$ excitation. The relation between the $4a_1$ intensity and the surface porosity is now well established. This is mandatory for the interpretation of the PSD-NEXAFS experiments studying the interaction of the ice surface with foreign molecules. Mainly, adsorption onto the pores will not change the $4a_1$ intensity, but only the continuum part of the PSD spectrum; conversely, adsorption on the flat portions of the surface will modify both the $4a_1$ and the continuum intensities.

(vii) Going from 38 to 147 K, the H_2O–H_2O distance at the surface increases from 2.77 to 2.80 Å, following an evolution that is dramatically different than for the bulk. Indeed, there is a continuous increase of this distance at the surface, whereas in the bulk, as said above, there is a steep change between 38 and 55 K and then no further changes between 55 and 147 K. It

is important to note that the H_2O–H_2O distance at the surface is systematically longer than in the bulk, and this difference increases with the temperature, certainly because at very low temperature the surface relaxation is hindered (and the structure of the bulk and of the unrelaxed surface are close), and relaxation proceeds as the thermal energy is given to the ice film. Thus, it is likely that at 147 K (and certainly at 160 K, where crystallization occurs), the surface relaxation is almost completed and the surface structure can be quite different from the bulk.

ACKNOWLEDGMENTS

The authors thank K. Le Guen, R. Guillemin, P. Morin, and M. Simon for their help during the recording of the H_2O gas-phase spectrum on the PAM6 experimental set-up.

[1] S. Solomon, R. R. Garcia, F. S. Rowland, and D. J. Wuebbles, Nature (London) **321**, 755 (1986).
[2] M. J. Molina, T. L. Tso, L. T. Molina, and F. C.-Y. Wang, Science **238**, 1253 (1987).
[3] L. d'Hendecourt and E. Dartois, Spectrochim. Acta, Part A **57**, 669 (2001), and references therein.
[4] P. Jenniskens and D. F. Blake, Science **265**, 753 (1994).
[5] J. E. Schaff and J. T. Roberts, J. Phys. Chem. **100**, 14151 (1996).
[6] X. Wei, P. B. Miranda, and Y. R. Shen, Phys. Rev. Lett. **86**, 1554 (2001).
[7] M. A. Zondlo, T. B. Onasch, M. S. Warshawsky, M. A. Tolbert, G. Mallick, P. Arenzt, and M. S. Robinson, J. Phys. Chem. B **101**, 10887 (1997).
[8] H. Ogasawara, N. Horimoto, and M. Kawai, J. Chem. Phys. **112**, 8229 (2000).
[9] B. Rowland, N. S. Kadagathur, J. P. Devlin, V. Buch, T. Feldman, and M. J. Wojcik, J. Chem. Phys. **102**, 8328 (1995).
[10] C. Manca, P. Roubin, and C. Martin, Chem. Phys. Lett. **330**, 21 (2000).
[11] N. Materer, U. Starke, A. Barbieri, M. A. Van Hove, G. A. Somorjai, G.-J. Kroes, and C. Minot, J. Phys. Chem. **99**, 6267 (1995).
[12] N. Materer, U. Starke, A. Barbieri, M. A. Van Hove, G. A. Somorjai, G.-J. Kroes, and C. Minot, Surf. Sci. **381**, 190 (1997).
[13] J. Braun, A. Glebov, A. P. Graham, A. Menzel, and J. P. Toennies, Phys. Rev. Lett. **80**, 2638 (1998).
[14] A. Lied, H. Dosch, and J. H. Bilgram, Phys. Rev. Lett. **72**, 3554 (1994); H. Dosh, A. Lied, and J. H. Bilgram, Surf. Sci. **327**, 145 (1995); Surf. Sci. **366**, 43 (1996).
[15] E. Mayer and R. Pletzer, Nature (London) **319**, 298 (1986).
[16] K. P. Stevenson, G. A. Kimmel, Z. Dohnalek, R. S. Smith, and B. D. Kay, Science **283**, 1505 (1999).
[17] R. J. Speedy, P. B. Debenedetti, R. S. Smith, C. Huang, and B. D. Kay, J. Chem. Phys. **105**, 240 (1996).
[18] R. S. Smith, C. Huang, E. K. L. Wong, and B. D. Kay, Phys. Rev. Lett. **79**, 909 (1997).
[19] R. S. Smith and B. D. Kay, Nature (London) **398**, 788 (1999).
[20] V. Sadchenko, K. Knutsen, C. F. Giese, and W. R. Gentry, J. Phys. Chem. B **104**, 2511 (2000).
[21] D. E. Brown, S. M. George, C. Huang, E. K. L. Wong, K. B. Rider, R. S. Smith, and B. D. Kay, J. Phys. Chem. **100**, 4988 (1996).
[22] M. S. Westley, G. A. Baratta, and R. A. Baragiola, J. Chem. Phys. **108**, 3321 (1998).
[23] M. T. Sieger and T. M. Orlando, Surf. Sci. **390**, 92 (1997).
[24] M. T. Sieger and T. M. Orlando, Surf. Sci. **451**, 97 (1997).
[25] W. C. Simpson, M. T. Sieger, T. M. Orlando, L. Parenteau, K. Nagesha, and L. Sanche, J. Chem. Phys. **107**, 8668 (1997).
[26] R. Azria, Y. Le Coat, M. Lachgar, M. Tronc, L. Parenteau, and L. Sanche, Surf. Sci. **436**, L671 (1999).
[27] E. Vichnevetski, A. D. Bass, and L. Sanche, J. Chem. Phys. **113**, 3874 (2000).
[28] R. Azria, Y. Le Coat, M. Lachgar, M. Tronc, L. Parenteau, and L. Sanche, Surf. Sci. **451**, 91 (2000).
[29] R. A. Rosenberg, P. R. LaRoe, V. Rehn, J. Stöhr, R. Jaeger, and C. C. Parks, Phys. Rev. B **28**, 3026 (1983).
[30] B. X. Yang and J. Kirz, Phys. Rev. B **36**, 1361 (1987).
[31] J. S. Tse, K. H. Tan, and J. M. Chen, Chem. Phys. Lett. **174**, 603 (1990).
[32] K. R. Wilson, J. G. Tobin, A. L. Ankudinov, J. J. Rehr, and R. J. Saykally, Phys. Rev. Lett. **85**, 4289 (2000).
[33] D. Coulman, A. Puschmann, U. Höfer, H.-P. Steinrück, W. Wurth, P. Feulner, and D. Menzel, J. Chem. Phys. **93**, 58 (1990).
[34] R. Romberg, S. P. Frigo, A. Ogurtsov, P. Feulner, and D. Menzel, Surf. Sci. **451**, 116 (2000).
[35] K. Mase, M. Nagasono, S. Tanaka, T. Urisu, E. Ikenaga, T. Sekitani, and K. Tanaka, J. Chem. Phys. **108**, 6550 (1998).
[36] K. Mase, M. Nagasono, and S. Tanaka, J. Electron Spectrosc. Relat. Phenom. **101–103**, 13 (1999).
[37] K. Mase, S. Tanaka, S. Nagoaka, and T. Urisu, Surf. Sci. **451**, 143 (2000).
[38] F. Bournel, C. Mangeney, M. Tronc, C. Laffon, and Ph. Parent, Phys. Rev. B **65**, 201404(R) (2002).
[39] F. Bournel, C. Manageney, M. Tronc, C. Laffon, and Ph. Parent, Surf. Sci. (to be published).
[40] J. Schirmer, A. B. Trofimov, K. J. Randall, J. Feldhaus, A. M. Bradshaw, Y. Ma, C. T. Chen, and F. Sette, Phys. Rev. A **47**, 1136 (1993).
[41] D. E. Ramaker, Chem. Phys. **80**, 183 (1983).
[42] A. Hiraya, K. Nobusada, M. Simon *et al.* Phys. Rev. A **63**, 042705 (2001).
[43] G. H. F. Diercksen, W. P. Kraemers, T. N. Resigno, C. F. Bender, B. V. McKoy, S. R. Langhoff, and P. W. Lanhoff, J. Chem. Phys. **76**, 1043 (1982).
[44] D. Menzel, G. Rocker, D. Coulman, P. Feulner, and W. Wurth, Phys. Scr. **41**, 588 (1990).
[45] P. Feulner and D. Menzel, in *Laser Spectroscopy and Photochemistry on Metal Surfaces (Part II)*, edited by H.-L. Dai and W. Ho, Advanced Series in Physical Chemistry, Vol. 5 (World Scientific Publishing, Singapore, 1995), p. 627.
[46] A. Naves de Brito, R. Feifel, A. Mocellin, A. B. Machado, S. Sundin, I. Hjelte, S. L. Sorensen, and O. Björneholm, Chem. Phys. Lett. **309**, 377 (1999).
[47] M. N. Piancastelli, A. Hempelmann, F. Heiser, O. Gessner, A. Rüdel, and U. Becker, Phys. Rev. A **59**, 300 (1999); I. Hjelte, M. N. Piancastelli, R. F. Fink *et al.* Chem. Phys. Lett. **334**, 151 (2001).
[48] J. P. Devlin and V. Buch, J. Phys. Chem. B **101**, 6095 (1997), and references therein.
[49] D. E. Ramaker, T. E. Madey, R. L. Kurtz, and H. Sambe, Phys. Rev. B **38**, 2099 (1988).
[50] J. Stöhr, in *NEXAFS Spectroscopy*, edited by R. Gomer, Springer Series in Surface Sciences, Vol. 25 (Springer-Verlag, Berlin-Heidelberg-New York), p. 242.
[51] J. Stöhr, in *NEXAFS Spectroscopy*, edited by R. Gomer, Springer Series in Surface Sciences, Vol. 25 (Springer-Verlag, Berlin-Heidelberg-New York), p. 123.
[52] A. L. Ankudinov, B. Ravel, J. J. Rehr, and S. D. Conradson, Phys. Rev. B **58**, 7565 (1998).
[53] J. D. Bernal and R. H. Fowler, J. Chem. Phys. **1**, 515 (1933).
[54] A. H. Narten, C. G. Venkatesh, and S. A. Rice, J. Chem. Phys. **64**, 1106 (1976).
[55] K. R. Wilson, B. S. Rude, T. Catalano, R. D. Shaller, J. G. Tobin, D. T. Co, and R. J. Saykally, J. Phys. Chem. B **105**, 3346 (2001).
[56] M. T. Sieger, W. C. Simpson, and T. M. Orlando, Phys. Rev. B **56**, 4925 (1997).
[57] V. Buch, J. Chem. Phys. **96**, 3814 (1992).